A&A 443, 211–222 (2005)
DOI: 10.1051/0004-6361:20052844

Astronomy & Astrophysics

Men'shchikov, A.B., & Miroshnichenko, A.S. 2005. A&A, 443, 211-222.
Properties of galactic B[e] supergiants. V. Two-Dimensional Radiative Transfer Model of RY Sct and its Dusty Disc.
Made available courtesy of EDP Sciences: http://dx.doi.org/10.1051/0004-6361:20052844

Properties of galactic B[e] supergiants

V. Two-dimensional radiative transfer model of RY Sct and its dusty disc

A. B. Men'shchikov[1,2] and A. S. Miroshnichenko[2,3,4]

[1] Institute for Computational Astrophysics, Saint Mary's University, Halifax, NS B3H 3C3, Canada
e-mail: amenshch@ap.stmarys.ca
[2] Max-Planck-Institut für Radioastronomie, Auf dem Hügel 69, 53121 Bonn, Germany
[3] Ritter Observatory, Department of Physics and Astronomy, University of Toledo, Toledo, OH 43606-3390, USA
[4] Central Astronomical Observatory of the Russian Academy of Sciences at Pulkovo, 196140, Saint-Petersburg, Russia

Received 8 February 2005 / Accepted 23 June 2005

ABSTRACT

We present results of the first two-dimensional radiative transfer modelling of the eclipsing binary RY Sct and its dusty disc. Assuming an effective temperature $T_\star = 27\,000$ K for both components and the distance $D = 1.8$ kpc, we derive the total luminosity $L_\star = 4.2 \times 10^5\,L_\odot$. The optically thin dusty disc ($\tau_V \approx 0.04$ in the equatorial plane) extends from its inner boundary at $R_1 = 60$ AU to the distances of $R_2 \approx 10^5$ AU, where it blends into the interstellar medium. The very high energy output of the supergiants heats up the interstellar dust, well beyond the outer boundary, to temperatures of ~ 100 K. It is the large interstellar extinction towards RY Sct ($A_V = 4.5$ mag) that defines its spectral energy distribution in the ultraviolet, optical and near infrared. The disc has a full opening angle $\psi = 26°$ and we observe it at a viewing angle $\theta_v = 14°$ from its midplane (inclination $i = 76°$). There is a strong density enhancement in the disc within a narrow ring at $r = 1500$ AU, that emits most of the infrared flux and is prominent in Keck telescope images (Gehrz et al. 2001, ApJ, 559, 395). The dust mass contained in the disc within 1″ from the star ($r < 1800$ AU) is $m_d = 3.2 \times 10^{-7}\,M_\odot$, by a factor of 3 lower than in previous estimates. However, in our model there is ~30 times more mass in the surroundings of the binary system than within the dense ring. As much as 95% of the total dust mass $M_d = 9 \times 10^{-6}\,M_\odot$ and gas mass $M = 0.017\,M_\odot$ of the circumbinary material is contained in the outer, old wind at $1800 < r < 10^5$ AU. Presumably the dense ring has been created by a fast wind that swept out and compressed the previously lost material in the older and slower stellar wind. Based on the new Keck data, our model predicts that presently there is a relatively large number of small, hot dust grains in the dust formation zone, whose emission substantially changes the shape of the SED of RY Sct in the near infrared. This suggests a higher mass-loss rate or dust-to-gas mass ratio or lower wind velocity, or a combination of these factors.

Key words. stars: emission-line, Be – stars: individual: RY Sct – stars: circumstellar matter – radiative transfer

1. Introduction

RY Sct is an eclipsing binary with a strong infrared (IR) excess produced by the circumstellar dust. The system has been studied in detail by different techniques. Multicolour optical light curves analyzed by different authors (e.g., Milano et al. 1981; Zakirov 1985; Antokhina & Cherepashchuk 1988; Antokhina & Kumsiashvili 1999; Djurasevic et al. 2001) clearly suggest that both companions are massive stars. However, there is no agreement in the literature on just *how* massive they are, with the estimates of the components' masses being in the range of 8–50 $M_\odot$, depending on the adopted mass ratio $q = M_{\star 2}/M_{\star 1}$ (3.3 or 1.25). Estimates of the orbital inclination angle i varied between 73° and 85°, the latter usually being associated with the high end of the mass range. The derived bolometric energy output of the binary system also widely differs (6–60 $\times 10^5\,L_\odot$), from well below the Eddington luminosity (Djurasevic et al. 2001) to several times above it (King & Jameson 1979; Milano et al. 1981). The proposed physical types of the close binary include both a semi-detached (Cowley & Hutchings 1976) and an overcontact (Milano et al. 1981; Djurasevic et al. 2001) system, or one with the secondary component embedded in an opaque, geometrically thick disc (Antokhina & Cherepashchuk 1988; Antokhina & Kumsiashvili 1999).

The system is surrounded by a nebula containing significant amounts of gas and dust and emitting both emission lines and thermal IR radiation. In particular, the object exhibits many strong forbidden lines (e.g., [O I], [N II], [S III], and [Fe II], de Martino et al. 1992) that, in combination with the near-IR excess, puts it in the list of peculiar Be or B[e] stars (Allen & Swings 1976). According to the scheme of Lamers et al. (1998), RY Sct can be classified as a B[e] supergiant as from

various observational estimates each companion's luminosity is at least $\sim 3 \times 10^5\,L_\odot$. There is general agreement concerning the distance towards the object ($D \approx 2$ kpc) recently strengthened by the kinematic data (Smith et al. 2002).

A relatively strong optical emission-line spectrum and evidence for the presence of only warm (hotter than 150–200 K) dust in the system allow us to classify it as a member of the group of B[e] stars with warm dust (B[e]WD, Miroshnichenko et al. 2002). This group comprises objects with masses of $M_\star \approx$ 3–40 $M_\odot$ and luminosities of $\log(L/L_\odot) \approx 2.5$–5.1 that show a steep decrease of the mid-IR flux towards longer wavelengths. The evolutionary state of these objects is not well-constrained yet. They may still be on the main sequence or have recently finished this stage. A few B[e]WD stars are definitely supergiants, and have been found or are suspected to be binary systems (e.g., HDE 327083, MWC 300, Miroshnichenko et al. 2003, 2004). RY Sct fits very well into this subgroup.

At the same time, RY Sct is the most well-observed object among B[e]WD stars. Recently Gehrz et al. (2001) obtained IR images of the system with the Keck telescope and resolved the nebula at wavelengths 3–20 μm. These authors estimated the amount of dust in the system ($M_\mathrm{d} \approx 1.4 \times 10^{-6}\,M_\odot$), but did not model in detail the observed optically thin torus. Such a modelling is important for a better understanding of the object's physical properties and of dust formation around hot stars in general. So far, a theoretical explanation has been presented for dust formation only around extremely luminous objects, such as Wolf-Rayet (WR) stars and massive supergiants (e.g., Williams et al. 2001; Kraus & Lamers 2003). These objects are naturally capable of developing a strong radiatively-driven mass loss, which can easily account for high gas densities in the dust formation zone. A high optical depth shields more distant parts of the wind, so that dust can form closer to the star, at distances where the temperature of the optically-thin part of the wind would still be above the dust condensation temperature. Dust can also form in clumpy and/or colliding winds of the WR binaries. The dust formation in the luminous B[e]WD binaries can be similar to the above scenarios. However, it is not yet clear if this is the case for less luminous objects.

Since no other B[e]WD star has been observed in such detail as RY Sct, the Keck images of this system, combined with all other published information, provide a good opportunity to begin an observational study of dust formation in these objects and to place better constraints on the properties of the system from accurate radiative transfer calculations. In this work we applied two-dimensional (2D) radiative transfer modelling to derive physical parameters of the stars and circumbinary dust in RY Sct. The observational data used are described in Sect. 2, the model assumptions and derived parameters are presented in Sect. 3, the results are discussed in Sect. 5, and the overall summary of this work is given in Sect. 6.

2. Observational data

In order to constrain the parameters of RY Sct and its dusty environment, we collected published photometric broadband data in the range of λ 0.3–25 μm. They were further supplemented by the International Ultraviolet Explorer (IUE) data

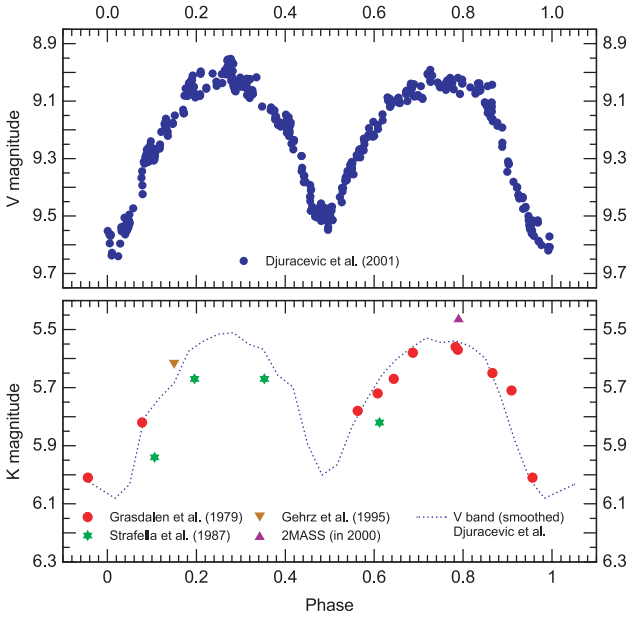

Fig. 1. The V- and K-band light curves of RY Sct. Photometric data from the papers quoted in the figure are shown by different symbols. The averaged V curve (shifted by 3.5 mag) is shown by a dashed line in the lower panel for comparison. The phases were calculated using the ephemeris from Djurasevic et al. (2001).

(λ 0.1–0.3 μm) taken from the INES archive and the Keck images and aperture photometry from Gehrz et al. (2001). The mid-IR (8–25 μm) data for RY Sct were taken from the Infrared Astronomical Satellite (IRAS) and Midcourse Space Experiment (MSX) Point Source Catalogs (IRAS PSC 1988; Egan et al. 2003). The object was detected in two IRAS bands (at 12 and 25 μm) and in four MSX bands (at 8.28, 12.13, 14.65, and 21.34 μm). The IRAS low-resolution spectrum exhibiting strong 10 μm silicate emission was taken from Volk & Cohen (1989). Co-addition of all IRAS scans (with the ADDSCAN procedure) through the position of RY Sct shows that the background radiation in the IRAS 60 and 100 μm bands is very complicated, and no point source can be detected there. Only sources with 60 μm fluxes brighter than ~60 Jy were detected in the 5 arcmin region around RY Sct. This is indirect evidence of the absence of noticeable amounts of cold dust ($T_\mathrm{d} \lesssim 100$ K) around the object.

Since the binary is eclipsing and its flux varies by $\Delta m \approx$ 0.6 mag shortward of $\lambda \approx 2\,\mu$m (by $\Delta m \approx 0.3$ mag in the L band at $\lambda = 3.6\,\mu$m), we used maximum fluxes in the $UBVRJHKL$ bands (at the orbital phases $\phi = 0.2$–0.25) to construct the observed spectral energy distribution (SED). Analysis of the published optical photometry obtained in 1970–1990s (e.g., Ciatti et al. 1980; Djurasevic et al. 2001) shows that the brightness level variations do not exceed the scatter of data points (~0.05–0.07 mag). The low-resolution ultraviolet (UV) spectra, obtained by the IUE in 1978–1988 at different orbital phases, show flux variations by a factor of ~2 due to the eclipses in the system. The strongest fluxes were detected on September 23, 1979 ($\phi = 0.72$). We added 10% to these fluxes in order to bring them to the brightest level (at $\phi =$ 0.2–0.25). Some near-IR observations of RY Sct showed fluxes

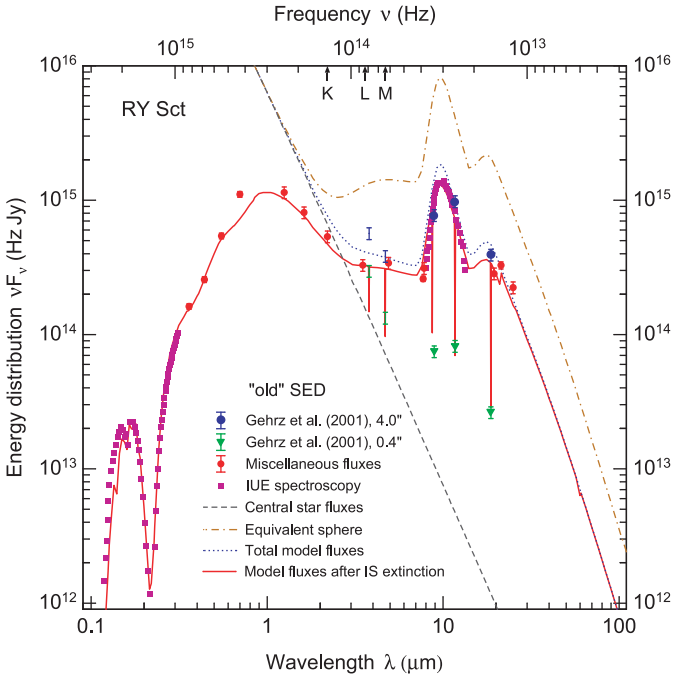

Fig. 2. Comparison of the model SED of RY Sct with the *old* photometric data. This fit to the observations ignores the *new* Keck telescope fluxes at 3.8 and 4.7 μm (shown by only error bars, without data points), because they imply a different density distribution (see Fig. 4). Assuming the distance of $D = 1.8$ kpc, our model predicts the total combined luminosity of $L_\star = 4.2\times10^5\,L_\odot$. The stellar continuum for $T_\star = 27\,000$ K, the total and beam-matched model fluxes without interstellar reddening, the model fluxes reddened by the interstellar extinction, and SED for an equivalent spherical envelope are plotted. Three arrows at the top axes indicate the locations of the K, L, and M photometric bands. The model assumes that we observe the disc close to edge-on orientation, at $\theta_v = 14°$. The effect of small 0.″4 beam sizes is shown by the vertical lines, clearly visible in the model SED at three Keck wavelengths (8.9, 11.7, and 18.7 μm). Whereas only the lower points of the vertical lines are relevant, we have connected them to the adjacent continuum by straight lines, to better visualize the beam effect that dramatically reduces the observable fluxes and makes them consistent with the small-beam Keck data. The shapes of the short-wavelength SEDs ($\lambda < 1\,\mu$m) in this and next figure are produced by the interstellar extinction.

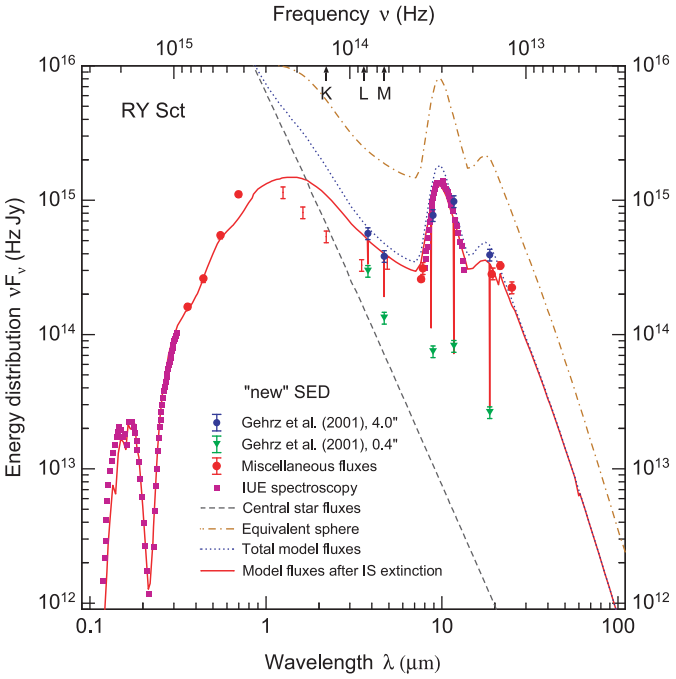

Fig. 3. Comparison of the model SED of RY Sct with the *new* photometric data. This fit to the observations ignores the *old* 1.25–3.5 μm fluxes (shown by only error bars, without data points), because they require a different density distribution, with larger amounts of hot grains (see Fig. 4b). The effect of small 0.″4 beam sizes in the model SED (vertical lines) is shown here at all five Keck wavelengths (3.8, 4.7, 8.9, 11.7, and 18.7 μm). See also caption of Fig. 2 for more details.

exceeding the light curve maximum shown in Fig. 1 (e.g., Allen 1973; Cutri et al. 2003). This suggests that the mass-loss rate or dust formation was variable in the past (see also Sect. 5).

Note that an analysis of the system's radio emission by Gehrz et al. (1995) suggested that the free-free contribution must be almost by two orders of magnitude lower than the observed fluxes of RY Sct in the entire range from optical to far-IR wavelenghts. This fact allows us to neglect the radiation of the ionized gas component in our dust continuum calculations.

3. The radiative transfer model

In order to derive more accurate physical parameters of RY Sct, we performed extensive numerical modelling of the system. To reduce large uncertainties even in the main parameters (such as the luminosity), it is necessary to model the object in detail. Although the dust emission is clearly optically thin, such modelling is able to constrain the parameters much better than usual simple estimates that had been applied to the object before.

Our analysis of the SED and IR images of RY Sct led us to the conclusion that the environment of the central binary is *non-stationary*. In fact, some of the λ 1–4 μm fluxes observed in the past are inconsistent with a factor of ~2 higher fluxes measured recently with the Keck telescope. The rapid evolution implied by the changes requires a quasi-time-dependent radiative transfer modelling, of the type that has been recently applied by Men'shchikov et al. (2002) to the quickly evolving environment of the carbon star IRC+10 216.

In the present study, we had to construct two models that describe the state of the dusty circumbinary environment of RY Sct and its SED at two epochs, in this paper referred to as "old" and "new". For the old data set we used the *JHKL* observations from Grasdalen et al. (1979) and Strafella et al. (1987), while for the new one we used the Keck data from Gehrz et al. (2001). The *UBVR* data for both SEDs and orbital ephemeris were taken from Djurasevic et al. (2001). The IUE and IRAS data were used for the UV and mid-IR parts of the observed SED of RY Sct shown in Figs. 2 and 3.

3.1. Geometry and assumptions

Our 2D continuum radiative transfer code (Men'shchikov & Henning 1997) employs a disc-like density distribution and an arbitrary number of dust components and grain sizes. The disc geometry is essentially the one depicted by Men'shchikov & Henning (1997) in their Fig. 1; our model of RY Sct is a

Table 1. Model parameters of RY Sct and its circumbinary disc. The radii of the binary components given here are the *effective* values computed with the assumptions that both stars are spherical, $T_{\star 1} = T_{\star 2}$ (= $T_\star$), and $R_{\star 1} = R_{\star 2}$ (= $R_\star$).

Parameter	Symbol	Value	Units	Uncertainty	Comment
Distance	D	1800	pc	±10%	assumed (from the literature)
Binary's total luminosity	$L_\star$	4.2×10^5	$L_\odot$	±30%	model (from fit to SED and distance, see also Sect. 5.2)
Effective temperatures	$T_\star$	27 000	K	±15%	assumed (from the literature, see also Sect. 5.1)
Effective stellar radii	$R_\star$	21	$R_\odot$	±10%	model ($R_\star = 2^{-1/2}(4\pi\sigma)^{-1/2} L_\star^{1/2}\, T_\star^{-2}$)
Inner boundary	R_1	60	AU	—	model ($R_1 \approx 150\, R_\star$, for carbon grains at $T_1 = 1700$ K)
Outer boundary	R_2	10^5	AU	—	assumed ($n_{\rm H} = 2$ cm$^{-3} \approx$ ISM gas density)
Location of dense ring	$R_{\rm r}$	1500–1800	AU	± 5%	model (from fit to the Keck telescope images)
Mass of dust disc	$M_{\rm d}$	9.0×10^{-6}	$M_\odot$	—	model (from fit to SED and model images, Sect. 5.4)
Total mass of disc	M	1.7×10^{-2}	$M_\odot$	—	model (corresponds to $\rho_{\rm d}/\rho = 5.3 \times 10^{-4}$)
Mass of dust disc ($r < 1''$)	$m_{\rm d}$	4.7×10^{-7}	$M_\odot$	—	model (from fit to SED and model images)
Total mass of disc ($r < 1''$)	m	8.9×10^{-4}	$M_\odot$	—	model (corresponds to $\rho_{\rm d}/\rho = 5.3 \times 10^{-4}$)
Dust temperature at R_1	T_1	1700	K	—	assumed (condensation of small carbon grains)
Dust temperature at R_2	T_2	130	K	—	model (small carbon grains at outer boundary)
Dust temperature at R_2	T_2	90	K	—	model (small silicate grains at outer boundary)
Density exponent 1	α_1	−9	—	—	model (60–130 AU)
Density exponent 2	α_2	−2	—	±20%	model (130–10^5 AU)
Equatorial optical depth	τ_V	0.043	—	±10%	model (from both fit to SED and model images)
Disc opening angle	ψ	26	°	±10%	model (from fit to the Keck telescope images)
Viewing angle	$\theta_{\rm v}$	14	°	±10%	model (from both fit to SED and model images)

relatively thin disc viewed slightly above its upper surface. The disc thickness is proportional to r (the radial distance from the central binary), so that the upper and lower disc surfaces form cones with the origin at the stars' center of mass. The full opening angle of the disc (between the upper and lower surfaces) in our final model was fixed at $\psi = 26°$ and the inclination of the disc midplane to the line of sight (the viewing angle) was found to be $\theta_{\rm v} = 14°$. The disc density distribution is essentially a 1D function of the radial distance from the center, $\rho = \rho\,(r)$. There is no dust above and below the disc surfaces in our model.

3.2. Physical parameters

The physical parameters of our model of RY Sct are listed in Table 1. Only the distance D and effective temperatures $T_\star$ are based on observational estimates found in the literature; other parameters are derived in our modelling. We assume that the distance is well determined by various observational methods and adopt a value of $D = 1.8$ kpc. For the distance, our modelling gives the total luminosity of the close binary of $L_\star = 4.2 \times 10^5\, L_\odot$, assuming that both hot stars are spherical and have identical $T_\star = 27\,000$ K; in this case, their *effective* radii are $R_\star = 21\, R_\odot$. The exact mass ratio and individual radii of the stars are irrelevant in our modelling, as long as the size of the binary is much smaller than the inner boundary of the dusty envelope. Note that our model luminosity is roughly an order of magnitude lower than the values adopted in several other works (e.g., Milano et al. 1981; Gehrz et al. 1995; Smith et al. 1999; Gehrz et al. 2001). See Sect. 5 for more discussion of the physical parameters.

In this study, we utilized several spherical atmosphere models with effective temperatures between 25 000 and 37 000 K, solar metallicity and gravity log $g = 2.5$–4.0. Several models were computed for us by Ian Short using the Phoenix code (Short & Hauschildt 2005) and some of the Kurucz (1993) atmospheres were also utilized. The original theoretical spectra were smoothed to a resolution of $\lambda/\Delta\lambda \sim 300$ and extrapolated to wavelengths $\lambda > 160\,\mu$m. In the final model, described below, we adopted an atmosphere with $T_\star = 27\,000$ K and log $g = 3.0$. This choice is discussed in more detail in Sect. 5.1.

The simplest possible dust model was adopted in this work, since no reliable information on the dust properties in RY Sct is available, except for the clear presence of amorphous silicates. The disc model contains small carbon grains ($a = 0.005\,\mu$m) and significantly larger silicate grains with a size distribution $\mathrm{d}n/\mathrm{d}a \propto a^{-3.5}$ for grain radii $0.05\,\mu\mathrm{m} < a < 1\,\mu$m. Optical constants for various laboratory analogs of cosmic dust were utilized to identify the dust grain materials that best fit the observations of RY Sct. The optical constants for carbon sample cel600 (Jäger et al. 1998) and astronomical silicates (Draine 1987) were found to give the best results. We adopted 2.0 g cm^{-3} and 3.3 g cm^{-3} as the grain material densities. To compute the size- and wavelength-dependent absorption and scattering efficiencies, $Q_{\rm abs}(a, \lambda)$ and $Q_{\rm sca}(a, \lambda)$, we used the Mie theory for spherical homogeneous particles.

The inner boundary of the disc is set by the condensation temperature of the most refractory (carbonaceous) component of dust grains. The latter was assumed to be $T_1 = 1700$ K and, accordingly, the inner boundary of the dust disc is at radius $R_1 = 60$ AU ($\approx 150\, R_\star$). Although no observational or physical constraints exist for the location of the outer boundary, it is quite reasonable to assume that dust must be present all the way into the interstellar medium. Thus, we fixed the outer boundary at $R_2 = 10^5$ AU, where the density of the circumbinary material drops to the interstellar level (∼1 H atom per cm^3).

The mass of gas and dust in the entire disc is only $M \approx 0.017\,M_\odot$, assuming the total dust-to-gas mass ratio $\rho_d/\rho = 5.3 \times 10^{-4}$ (of both dust components), constrained by the solar cosmic abundances of silicon and magnesium. Our model requires carbon grains to be much less abundant than the silicates, with $\rho_C/\rho = 3.45 \times 10^{-5}$. The density distribution in the model follows the spherical constant-velocity outflow profile $\rho \propto r^{-2}$ with a density enhancement by a factor of ~40 at the location of the toroidal ring, seen in the Keck images of RY Sct. The density distribution (mass-loss rate) is non-stationary, and at present the density profile is very steep ($\rho \propto r^{-9}$) in the vicinity of its inner boundary (see discussion in Sect. 5.4).

The dusty disc is optically thin ($\tau_V \approx 0.04$ in the equatorial plane), so it is mainly the large interstellar extinction of $A_V = 4.50$ mag towards RY Sct that defines its SED at the UV, optical, and near IR. The extinction was taken into account by reddening the model fluxes using the analytic fits by Cardelli et al. (1989), extended to $\lambda = 100\,\mu$m with the data from Savage & Mathis (1979), and parameters $R_V = 3.4$ and $n_H = 1.52\,\mathrm{cm}^{-3}$. The latter correspond to the best-fit A_V at the distance D (see below).

3.3. Numerical parameters

The numerical model included 600 radial zones, 10 angular zones for the integration of the mean intensity, 50 angular zones for the observations of a converged model and 217 non-uniformly distributed frequencies (for details, see Men'shchikov & Henning 1997). The grain size distribution was binned into 19 representative grains. The iterations were terminated when relative corrections to all variables were below 0.001 % and the total energy was conserved to within 0.02 %.

4. Results of the modelling

4.1. Parameter space

The final parameters of our detailed radiative transfer model and their approximate uncertainties are presented in Table 1. The density distribution is assumed to be a broken power law $\rho \propto r^{\alpha_i}$, the exponents α_i ($i = 1, 2$) being allowed to change in different radial zones. The third column lists the values adopted in the final model. The fifth column contains our estimates of the uncertainties associated with the final model parameters. They indicate very approximately the maximum changes of the parameters, such that the fit to the observations can still be restored by adjusting some other model parameters (see also Table 3 and Sect. 5). The uncertainties should not be interpreted as absolute error bars. If some of our general assumptions turn out to be insufficiently realistic, this might possibly affect the results more than these uncertainties imply.

The results of our radiative transfer modelling are invariant with respect to the distance D, except for several parameters that are scaled in the following simple way:

$$L \propto D^2,\ M \propto D^2,\ R \propto D,\ \rho \propto D^{-1}, \quad (1)$$

where mass and density refer to the properties of dust; for conversion to the gas parameters, ρ_d/ρ must be specified (Sect. 3.2). These relations make it easy to scale the model results to another distance, if necessary.

4.2. Spectral energy distribution

Comparison of our model of RY Sct with its observed SED at two epochs is shown in Figs. 2 and 3; the corresponding density and temperature distributions are displayed in Fig. 4.

A careful inspection of Figs. 2–4 reveals that it is *impossible* to reproduce the *new* 3.8–4.7 μm fluxes and Keck telescope images of the disc simultaneously with the *old* 1.25–3.5 μm fluxes. Most obviously, this is demonstrated by the two fluxes at λ 3.5 and 3.8 μm. They are almost identical (within 5%), although the old flux had been measured in a large beam but the new flux was obtained in a much smaller 0.″4 aperture. This sharply contrasts with the fact that the Keck fluxes in large and small beams differ by almost a factor of 2 at 3.8 μm. There is no good reason to believe that either the old or the new data are in error and to ignore them. Even if one discards the 3.5 μm flux, there is no way to fit *any* dust emission through the large-beam 1.25–2.2 μm old fluxes and the large-beam 3.8–4.7 μm Keck fluxes (cf. Fig. 2). This is why the old and the new SEDs of RY Sct are mutually exclusive and our model predicts that at present its continuum must look like the one plotted in Fig. 3. This conclusion can easily be tested by new near-IR photometry of RY Sct at its maximum light.

We believe that the only way to reconcile these incompatible fluxes is to assume that the disc structure has changed between the observations. In the frame of our modelling, the only possible explanation is that relatively large amounts of small, hot ($T_d \gtrsim 1000$ K) dust grains have formed in the innermost regions of the disc since the old observations. This enhanced dust density may have resulted from increased gas density in the dust formation zone which, in turn, could have been caused by a recent episode of increased mass loss or perhaps by decreased outflow velocity (see also Sect. 5.4).

The pronounced beam effect in the Keck observations, with a factor of 2–10 smaller fluxes in a 0.″4 beam compared to the 4.″0 beam emphasizes the extended nature of the observed IR emission. Our model fits the SEDs of RY Sct at both epochs almost perfectly. Some deviation from the observed flux at λ 8.9 μm indicates that the observed 10 μm silicate feature is actually somewhat narrower than that of the astronomical silicates adopted in our modelling. Other than that, the astronomical silicates give the best fit to the SED of RY Sct among several other types of amorphous silicates we tried to use in the modelling.

4.3. Densities and temperatures

The density profile $\rho \propto r^{-2}$, adopted in this work everywhere except for the dense ring at $r = 1500$ AU (Fig. 4), is consistent with both the SED and the IR images of RY Sct. The steeply increasing density profile $\rho \propto r^{-9}$, $r \leq 130$ AU, towards the inner disc boundary at 60 AU (dust formation zone) is required

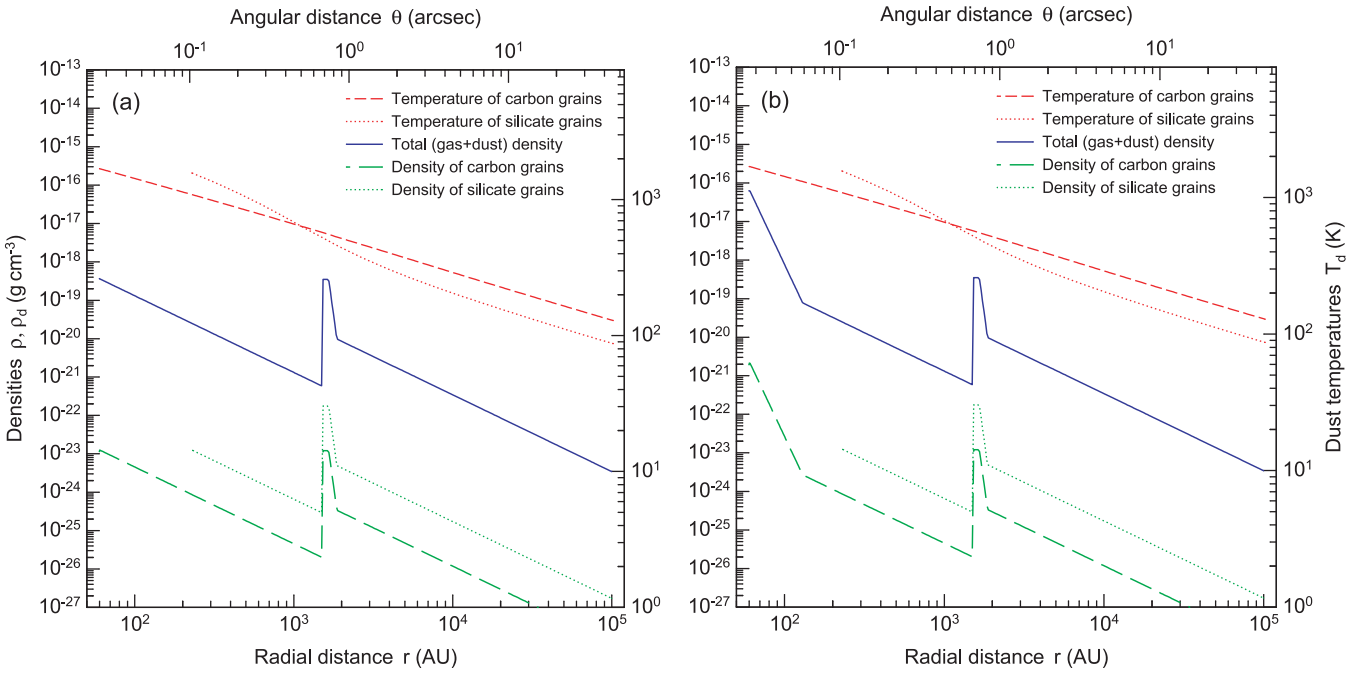

Fig. 4. The *old* **a)** and *new* **b)** disc structures, corresponding to the fits of the SEDs of RY Sct shown in Figs. 2 and 3, respectively. The density and temperature distributions are shown for only the smallest carbon and silicate grains with radii of 0.005 and 0.05 μm, respectively. As there are no observational constraints on the radial dependence of the dust-to-gas mass ratio, we had no other choice but to assume that $\rho_{\rm d}/\rho$ is constant both in space and time. This implies that the *gas* density profile follows that of the dust density, the latter being reconstructed by our model ($\rho \propto r^{-2}$ everywhere except the dense ring at 1500 AU and the dust formation zone with $\rho \propto r^{-9}$ at ~100 AU in panel **b)**.

by our model of RY Sct to reproduce the new SED (Fig. 3) and IR images (Fig. 5). The hot dust density must now be substantially higher in the dust formation zone, suggesting a much higher mass-loss rate or much lower wind velocities or a much higher dust-to-gas mass ratio than before, or a combination of these. See also discussion in Sect. 5.4.

The strong density peak in the disc within a narrow ring at $r \approx 1500$ AU emits most of the IR flux and is well visible in the Keck telescope images (Gehrz et al. 2001). The density contrast with the surroundings just inside and just outside of the peak is ~600 and 40, respectively. The dense ring is very much reminiscent of a shell that has been created by a fast wind that swept out and compressed the previously lost material in the older and slower stellar wind. Only a tiny fraction of $\sim 10^{-3}$ of the total disc mass is contained at $r < 1500$ AU, whereas 50 times more mass is contained within the dense ring itself. Still, as much as 95% of the total mass of 0.017 $M_{\odot}$ is contained in the outer, old wind material, at $1800 < r < 10^5$ AU.

The lack of the far-IR and submillimeter observations usually makes it harder to reconstruct the mass-loss history of a star. However, in the case of RY Sct, the steep decline of fluxes at $\lambda \gtrsim 20\,\mu$m contains almost no information either on the density distribution beyond the dense ring, or on the location of the outer edge of the dusty wind of RY Sct. This is because the dust temperatures remain quite high even at large distances from the very luminous central binary (Figs. 4 a,b). In fact, the dust temperatures are higher than 100 K everywhere up to the outer boundary at 10^5 AU. The shallow radial dependence of the dust temperatures ($T_{\rm d} \propto r^{-0.33}$) in this optically thin environment means that the temperatures remain above 50 K up to distances of $\sim 10^6$ AU. Thus, it is not surprising at all that only warm or hot dust is observed around the RY Sct binary and other supergiants with optically-thin envelopes, as their huge energy output heats up the circumstellar and interstellar dust within *many parsecs* of the stars.

4.4. Infrared images

The model infrared images and intensity profiles displayed in Figs. 5 and 6 are remarkably similar to the recent images of RY Sct obtained with the Keck telescope (Gehrz et al. 2001). This very good quantitative agreement confirms that our reconstruction of the model geometry and physical parameters is reliable.

Model images shown in Fig. 5 can be directly compared to the Keck images, as they were computed at the same wavelengths, convolved with similar point-spread functions (PSF) and have the same orientation. Obviously, there are some reasons why the comparison may only be approximate and qualitative. The observed images do not have the same degree of symmetry as in our model, we could not reconstruct the observed noise level and the colour coding and the model images are monochromatic, whereas the observed images were recorded using a finite filter profile. However, these differences play a minor role, and the agreement is very good.

To compare the model and observations in a more quantitative way, we extracted the intensity profiles from our images along the straight line through the central stars and both intensity peaks at the location of the dense ring. The intensity profiles shown in Fig. 6 can be directly compared to the

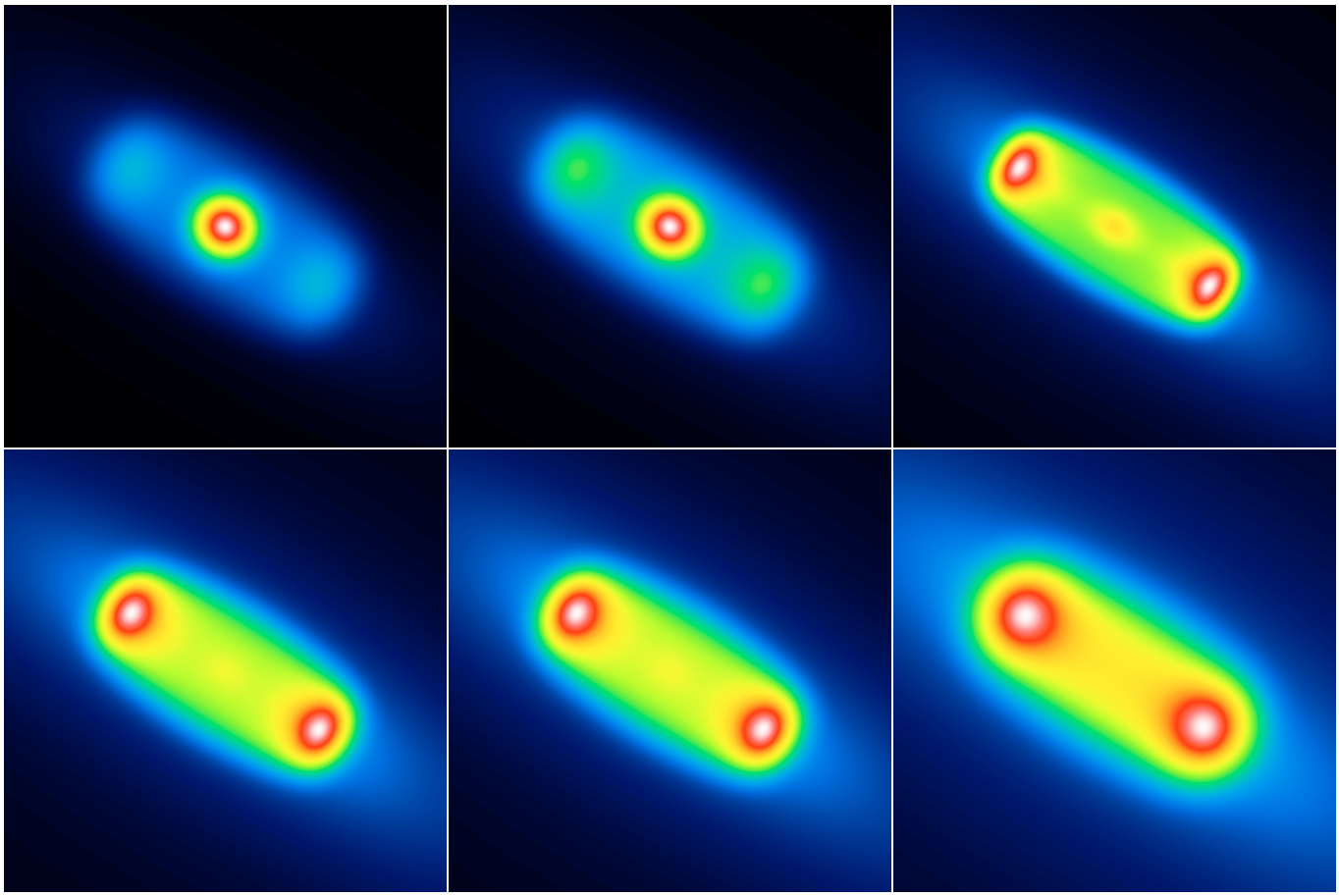

Fig. 5. Model images of RY Sct at 3.8, 4.7, 8.9, 11.7, 12.5, and 18.7 μm (*left to right, top to bottom*). The images can be directly compared to the raw Keck telescope images presented by Gehrz et al. (2001), although we did not attempt to recover their colour coding nor the lowest intensity level. The model images have the resolution (PSFs of 0.″25, 0.″25, 0.″3, 0.″3, 0.″19, 0.″25, 0.″27, and 0.″4, respectively), scaling (square root of intensity) and orientation (PA = 58°) of the observed images. The field of view of all images is $3.''2 \times 3.''2$. Comparison of the model and observed intensity slices through the images is shown in Fig. 6.

intensity scans presented by Gehrz et al. (2001) in their Fig. 5. Similarly to the images discussed above, there are some minor differences in the way the observed and model profiles were obtained. The model profiles are monochromatic, they do not account for the finite width of a narrow strip over which the observed intensity scans were integrated. In addition, we had to average the two arms of the observed profiles, as they are noticeably asymmetric, whereas our model is symmetric by construction.

Both the image and the intensity profile at 12.5 μm in our model are somewhat different from the observations also because RY Sct has an uncertain contribution from the [Ne II] emission at 12.8 μm that comes from the inner parts of the disc relative to the peaks (Gehrz et al. 2001). We believe that when added to our model image at this wavelength, the model intensity profile would agree much better with the observations.

5. Discussion

Our detailed 2D radiative transfer modelling of RY Sct presented in Sect. 4 allowed us to derive some physical properties of the binary and its dusty disc much more accurately and reliably than has been done before using only simple approximate estimates. Below, we discuss several aspects of our results in more detail.

5.1. Effective temperatures

The origin of the frequently quoted spectral classification of RY Sct as O6–O7 plus O9–B0 binary (Milano et al. 1981; de Martino et al. 1992; Gehrz et al. 1995; Smith et al. 2001) and high effective temperatures of its components ($T_\star$ of 37 000 and 30 000 K) can be traced to an IUE study by Koch (1979). Comparing dereddened spectra with model atmospheres, he concluded that $T_\star = 40\,000$ K and $3.5 < \log g < 5$ describe the 1350–3300 Å spectrum within the precision of the observations. As the quality of the spectra used was not very good, we regard this classification as fairly uncertain. Also on the basis of IUE spectra, Sahade et al. (1984) classified RY Sct as a B0 star ($T_\star = 30\,000$ K, $\log g = 4.0$) and in a recent detailed study, Sahade et al. (2002) confirmed this result.

A sensitive indicator of effective temperatures is the presence or absence of He II lines. It has been shown that in supergiants the He II 4686 Å line goes from absorption into emission

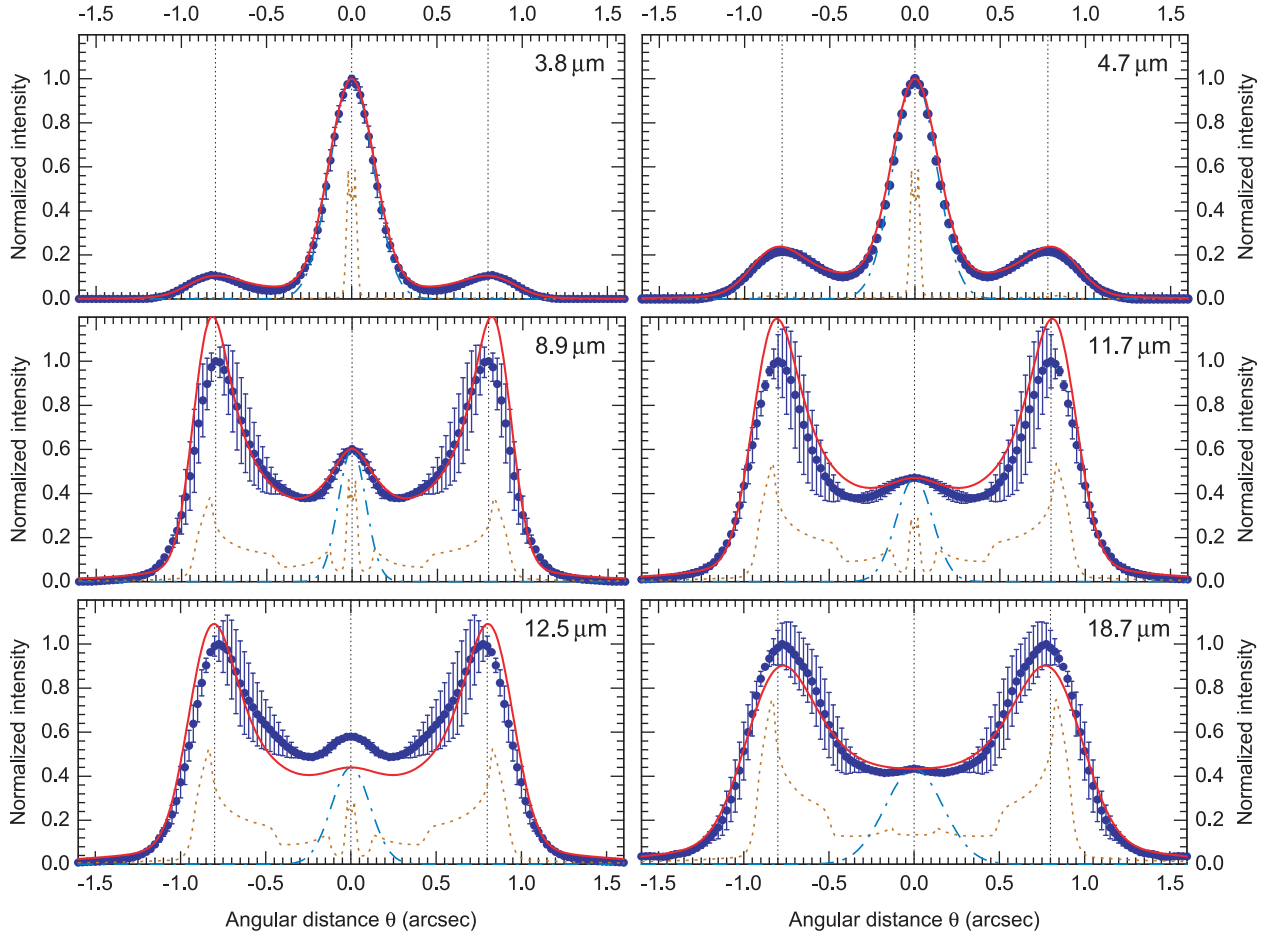

Fig. 6. Normalized intensity profiles of our model of RY Sct at 3.8, 4.7, 8.9, 11.7, 12.5, and 18.7 μm (solid lines) are compared to the observed intensity scans at the same wavelengths (filled circles) presented by Gehrz et al. (2001). As the observed profiles are asymmetric, whereas our model is symmetric by definition, we averaged the two observed arms and display the range of differences between them by vertical bars. Also shown are the profiles of the circular PSFs used in the model convolution (dash-dotted line), as well as the true, unconvolved, model intensity profiles (dotted line). The model profiles represent slices through the images displayed in Fig. 5. The central portion of the 12.5 μm model profile shows a deficit of radiation due to a contribution of the [Ne II] emission to the observed intensities.

with increasing temperatures at $T_\star \approx 28\,000$ K (Schmutz et al. 1991). Cowley & Hutchings (1976) found that the He II 4686 Å line was in emission in RY Sct, but it was weak and broad and its radial velocity curve was different from those of the binary components. They suggested that the line is formed between the stars and thus it gives no evidence that any of the companions is hotter than 27 000–28 000 K. Sahade et al. (2002) also noted that the He II 4686 Å line appears only as a weak broad emission, not consistent with its formation in the atmospheres of any of the companions. They concluded that the primary (B0 V) has a mass of 10 $M_\odot$ and the secondary component with 36 $M_\odot$ has an opaque disk, in which the He II line is formed.

Analyzing the *UBVR* light curves of RY Sct in the frame of the Roche model and assuming that its spectral type is close to B0, Djurasevic et al. (2001) found two possible sets of parameters, for $T_{\star 1} = 28\,000$ K, $T_{\star 2} \approx 24\,000$ K, and $T_{\star 1} = 30\,000$ K, $T_{\star 2} \approx 26\,000$ K. From that photometric solution they derived $\log g_1 \approx 2.7$, $\log g_2 \approx 2.8$ and the components' masses of 7.9 and 26 $M_\odot$, as well as concluded that the cooler secondary component dominates the binary's SED and that it has hotter spots on its surface.

Solving an inverse problem for the newly obtained *uvbyβ* light curves of RY Sct, Antokhina & Kumsiashvili (1999) concluded that the B0 star ($T_\star = 28\,000$ K) fills its Roche lobe and transfers mass onto the hotter secondary which is embedded in an opaque disc-like envelope (that has polar and equatorial temperatures of 43 000 and 19 000 K, respectively). The authors suggested that the binary (with the components' masses of 8 and 26 $M_\odot$) currently evolves into a WR + OB system.

All these observational data and estimates suggest that the real situation in this close binary system is very complex and uncertain. Even the concept of specific values $T_{\star 1}$ and $T_{\star 2}$ describing the effective temperatures of these strongly distorted ellipsoidal components of RY Sct, with inhomogeneous temperature distributions over their surfaces, may well be considered useless, at least for some applications.

Fortunately, the problem considered in this work can be easily simplified by replacing the close binary with a single energy source having luminosity $L_\star$ of the binary system and *effective* $T_\star$. Indeed, two individual SEDs of the binary components, each having a different luminosity and effective temperature, would appear to the distant dusty disc as a source of the

Table 2. Estimates of the basic physical parameters of the close binary RY Sct. Columns with $L_{\rm E}$ contain the Eddington luminosity; all other notation has its usual meaning. Two values of $T_{\star 2}$ marked by asterisks refer to the average temperatures over a thick accretion disc around the secondary component. Our model entries contain *effective* values obtained from the total luminosity of the binary (Table 1) assuming, for an illustration, that the components are the same and both have a mass of 20 $M_\odot$.

$T_{\star 1}$ (K)	$T_{\star 2}$ (K)	$L_{\star 1}$ ($L_\odot$)	$L_{\star 2}$ ($L_\odot$)	$L_{\rm E1}$ ($L_\odot$)	$L_{\rm E2}$ ($L_\odot$)	$R_{\star 1}$ ($R_\odot$)	$R_{\star 2}$ ($R_\odot$)	$M_{\star 1}$ ($M_\odot$)	$M_{\star 2}$ ($M_\odot$)	log g_1	i (°)	Reference
								36	46	3	80	Cowley & Hutchings (1976)
30 000		1.1×10^6		5.8×10^5	1.1×10^6	39.2		18	35	2.5		King & Jameson (1979)
32 000	43 000	1.6×10^6	4.4×10^6	1.6×10^6	1.3×10^6	40.6	36.7	48.9	39.1	2.9	73	Milano et al. (1981)
30 000	26 000	5.0×10^5		5.8×10^5	1.3×10^6	25		18	40	2.9	75	Giuricin & Mardirossian (1981)
28 000	26 000*	2.5×10^5	4.7×10^5	2.6×10^5	8.4×10^5			8	26		85	Antokhina & Cherepashchuk (1988)
30 000	37 000	1.2×10^6	2.2×10^6	1.6×10^6	1.3×10^6	40.6	36.7	48.9	39.1	2.9		Gehrz et al. (1995)
28 000	25 600*	2.4×10^5		2.6×10^5	8.4×10^5	21		8	26	2.7	85	Antokhina & Kumsiashvili (1999)
30 000	26 000	3.0×10^5	4.8×10^5	2.6×10^5	8.4×10^5	20.5	34.3	7.9	26.1	2.7	84	Djurasevic et al. (2001)
28 000	24 000	2.3×10^5	3.5×10^5	2.6×10^5	8.4×10^5	20.5	34.3	7.9	26.1	2.7	84	Djurasevic et al. (2001)
30 000				3.2×10^5	1.2×10^6			10	36		85	Sahade et al. (2002)
27 000	27 000	2.1×10^5	2.1×10^5	6.2×10^5	6.2×10^5	20.9	20.9	20	20	3.1		present model (effective values)

Table 3. Dependence of the model parameters of RY Sct and its circumbinary disc on the adopted stellar atmosphere model ($T_\star$ and log g). *Effective* radius $R_\star$ of the binary components (assuming they are equal) was derived from $L_\star$ and *effective* $T_\star$ (see formula in Table 1). Rows with BB in the log g column correspond to blackbody atmospheres.

$T_\star$ (K)	log g (cm s^{-2})	$L_\star$ ($L_\odot$)	$\Delta L/L$ (%)	$R_\star$ ($R_\odot$)	$\Delta R/R$ (%)	M ($M_\odot$)	$\Delta M/M$ (%)	τ_V (old)	τ_V (new)	$n_{\rm ISM}$ (cm^{-3})	Comment
25 000	3.3	3.40×10^5	−19	22.0	+5	0.019	+12	0.020	0.050	1.49	
25 000	BB	2.80×10^5	−33	19.9	−5	0.023	+35	0.024	0.059	1.45	
27 000	4.0	4.50×10^5	+7	21.6	−3	0.016	−6	0.017	0.041	1.50	
27 000	3.0	4.20×10^5	0	20.9	0	0.017	0	0.018	0.043	1.52	reference model values
27 000	2.5	4.00×10^5	−5	20.4	−2	0.018	+6	0.019	0.046	1.50	
27 000	BB	3.50×10^5	−17	19.1	−9	0.020	+18	0.021	0.051	1.47	
30 000	4.0	6.00×10^5	+43	20.3	−3	0.012	−29	0.013	0.031	1.55	
30 000	3.0	5.50×10^5	+31	19.4	−7	0.013	−24	0.014	0.033	1.54	
30 000	2.5	5.20×10^5	+ 24	18.9	−10	0.014	−18	0.014	0.033	1.52	
30 000	BB	4.80×10^5	+14	18.1	−13	0.015	−12	0.016	0.038	1.50	
37 000	4.0	1.05×10^6	+150	17.6	−16	0.007	−59	0.0077	0.019	1.585	
37 000	BB	8.50×10^5	+100	15.8	−24	0.009	−47	0.0096	0.023	1.535	

total luminosity with an *average* effective temperature. As even the disc's inner boundary is located at much greater distances than the separation of the components (by a factor of ∼200), it is clear that the accuracy of this approximation is definitely more than sufficient for our purpose of the radiative transfer modelling in the dusty disc of RY Sct.

The adopted value of $T_\star = 27\,000$ K for the central energy source in our model of RY Sct is a suitable average effective temperature considering all the recent observational estimates listed in Table 2. Our investigation of the model parameter space and dependence of the derived parameters on the adopted stellar atmosphere (Table 3) shows that related uncertainties of our results are ∼30% in total luminosity and disc mass and ∼10% in stellar radii.

5.2. Stellar luminosity

The total luminosity $L_\star = 4.2\times10^5\,L_\odot$ derived in our model of RY Sct is by factors of 14 and 8 lower than the values adopted by Milano et al. (1981) and Gehrz et al. (1995), respectively. At the same time, the new value is within a factor of 2 of all other estimates (Table 2). The previous estimates of very high luminosity of RY Sct (exceeding the Eddington limit) were based on the derived radii of the components of this eclipsing binary and their high effective temperatures. However, both the masses and radii of the stars are not very well constrained (Table 2), and thus they gave erroneous values. Our model value of $L_\star$ is quite reliable, since it is the primary parameter of a direct model fit to the observed SED, based on accurate radiative transfer calculations. Although it still somewhat depends on our assumption that both stars have the same $T_\star$ = 27 000 K, this value seems to be consistent with the observations (Sect. 5.1) and, besides, the uncertainties of $L_\star$ in our model are ∼30% (Table 3).

Note that the shape of the short-wavelength SED is produced purely by interstellar extinction. Using the well-known interstellar extinction law, we have only a little freedom in choosing two of its parameters, namely $R_V = 3.4$ and

$n_{\rm H} = 1.52$ cm^{-3}. The values are derived with a very good accuracy by the precise fit of the shape of the optical/UV continuum. The above number density of the interstellar H atoms is also consistent with our choice of the outer boundary of the dusty disc of RY Sct at $R_2 = 10^5$ AU, where the disc has $n_{\rm H} \approx 2$ cm^{-3}.

The very accurate model fit to the short-wavelength part of the SED ($\lambda < 1\,\mu$m) puts a very tight constraint on the luminosity of RY Sct. The absolute upper limit for $L_\star$ can be obtained by setting a very high value of $T_\star = 37\,000$ K, which in our modelling gives $L_\star^{\rm max} \approx 10^6\,L_\odot$ (Table 3). It is impossible to fit the SED with a higher luminosity. However, as the assumed $T_\star = 37\,000$ K seems to be unrealistically high, the limit is most likely closer to $L_\star^{\rm max} \approx 6 \times 10^5\,L_\odot$ (cf. Table 3). Note that the ionized region within the dusty ring of RY Sct should not influence our model results, as the free-free fluxes are by 2 orders of magnitude lower than those produced by the dust emission at all wavelengths of interest (Gehrz et al. 1995).

There remains some uncertainty in the luminosity of RY Sct also due to the uncertain geometry of the binary system. If the binary's secondary component is indeed a very hot star embedded in an opaque ellipsodial disc (Antokhina & Cherepashchuk 1988; Antokhina & Kumsiashvili 1999), then its radiation may be significantly anisotropic. In that case, a fraction of the total luminosity of the secondary can escape into the polar directions, avoiding detection, and thus the actual energy output of the binary may be higher than that implied by the observed fluxes. It is still unknown, however, whether the binary model describes the real binary accurately enough to attempt to take this effect into consideration. Our radiative transfer calculations assume isotropic radiation of the stars, as any other modelling of this kind.

5.3. Binary mass

Although our modelling does not constrain the binary's mass directly, the much lower total luminosity suggests significantly lower mass than the frequently quoted 80–90 $M_\odot$ suggested by Cowley & Hutchings (1976) and Milano et al. (1981). The existing mass estimates from the literature collected in Table 2 seem to indicate that the higher masses correlate with a smaller orbital inclination i obtained from solutions to the observed light curves. For an illustration, in Table 2 we assumed that our model binary has a mass of 40 $M_\odot$, which is half that of the most extreme values and in line with a number of other estimates. The luminosity of such a system is well below its Eddington limit.

If we were to assume that the binary orbit is coplanar with the model disc, its orbital inclination would be close to $i \approx 76°$ (Table 1). Although this orientation of our model disc corresponds to the lower end of the inclination range, the lower luminosity of the model seems to favor the lower mass of the binary, in an apparent contradiction to the trend. There would be no such difficulty if the orbit was not coplanar with the disc but inclined to its equator by roughly 10°, which cannot be excluded. Note, however, that the uncertainties in the orbital inclinations derived from light curves may well be large enough to bring even a coplanar orbit in agreement with the lower masses.

5.4. Dust and gas

Recent estimates of the dust mass in the disc (limited in size by the observed dense ring) gave $1.4 \times 10^{-6}\,M_\odot$ within a radius of 1″ (Gehrz et al. 2001). That mass is by a factor of 3 higher than the more accurate value of $m_{\rm d} = 4.7 \times 10^{-7}\,M_\odot$ derived in this work, which is by 30% lower than the older estimate of $6.5 \times 10^{-7}\,M_\odot$ (Gehrz et al. 1995). Moreover, our modelling strongly suggests that most of the circumbinary mass is contained in the outer regions of the old stellar wind, just *outside* the dense ring. In fact, the total mass of the dust in the binary's environment that can be attributed to its stellar wind is $M = 9 \times 10^{-6}\,M_\odot$, a factor of 6–14 higher than the previous estimates that neglected the presence of extended outer regions.

The choice of the density distribution in the inner regions of the dusty disc is somewhat arbitrary. In the absence of good observational constraints, we chose the simplest power-law forms of $\rho \propto r^{-2}$ and $\rho \propto r^{-9}$ that fit the data. The only two constraints are that the old inner density profile must not give any noticeable emission in the near IR and the enhanced dust emission of the new profile must reproduce the observed Keck fluxes and images at 3.8 and 4.7 μm. The density peak at the inner boundary must also be compact enough to remain unresolved by the Keck images. Clearly, there is a variety of possible profiles that conform to these constraints. Note that the modelling results are based on our assumption that both old and new fluxes are reliable. Given that, our conclusion about the enhanced dust density at the inner boundary of the disc is reliable, too.

The model requires that the disc outside the dense ring contains some material, based on our fitting of the Keck images. The low-level intensity profiles in Fig. 6 just outside the bright peaks imply the r^{-2} density profile displayed in Fig. 4. It is quite natural to expect that those distant parts of the binary environment were filled by the stellar wind during the long lifetime of the stars. Note, however, that our conclusions on the large scale density and mass distribution is based on the available mid-IR images probing only 3 arcsec around RY Sct. It is clear that new far-IR/submm observations with large beams are required to detect any material that might have been lost by the binary system long ago.

Carbon and silicate dust grains form at two distinct zones, corresponding to their condensation temperatures of ~1600–1700 K. In the optically-thin environment of RY Sct, the temperatures are attained at distances of 60 AU and 230 AU from the central binary. An idea that dust grains around RY Sct should exist (form) only in the dense ring at 1500 AU (Gehrz et al. 2001) is inconsistent with our modelling. In fact, the presence of new small, hot grains in the innermost parts of the disc is required to fit the Keck images and SED of RY Sct. Although we tried to use different grain materials, it was the carbon grains that gave the best fit to the data. There is insufficient information to uniquely constrain the dust material except that it must have steep IR emissivity to be consistent with the observations.

The system is considered to be close to the WR stage and the presence of a noticeable amount of carbon is not surprising, taking into account the evolved status and the mass exchange which should expose stellar interiors. Carbon lines are observed in the IUE spectrum of RY Sct (Sahade et al. 2002; Smith et al. 2002) and the near-IR imaging by Gehrz et al. (1995) suggested the presence of polycyclic aromatic hydrocarbons in the nebula. Thus, it is quite reasonable to add the carbon dust to the silicate dust component, although unlike the latter, carbon grains do not exhibit any feature in the observed continuum.

The models presented here imply that the central bright intensity peak, dominating the images at 3.8 and 4.7 μm, is *not* the direct light from the central stars, but rather the unresolved emission from a relatively dense region of hot grains just outside the carbon dust formation zone at $R_1 = 60$ AU. Our extensive, detailed fitting of the SED of RY Sct demonstrated that the stellar photospheres alone are not bright enough to produce the central peak. Note that the small-aperture fluxes derived from the Keck images are well above the stellar continuum in Figs. 2 and 3, by roughly a factor of 2. No acceptable fit of the observed SED and images could be found with the stars dominating the small-aperture fluxes. Thus, a firm conclusion from the modelling is that the central intensity peaks in the images are produced by relatively large amounts of new dust.

5.5. Other considerations

It is hard to speculate about the history of mass loss in RY Sct, given the rather small number of multiwavelength observations. Smith et al. (2001) mentioned that the object was described as having "very faint dark hydrogen lines" in the Henry Draper catalog (probably in the 1870s), but exhibited a bright Hβ emission in 1920s. These authors attribute the appearance of the circumstellar material to an S Dor type outburst of one of the companions and refer to a light curve of the system, which differs from the one published by Gaposhkin (1937). A careful inspection of figures from Gaposhkin's paper shows that Smith et al. (2001) confused RY Sct with R CrA due to a different order of the figures and their captions. The real light curve of RY Sct, shown by Gaposhkin, is very similar to the modern one, except for a larger difference between the primary and secondary minimum (~0.3 mag in 1920s and ~0.1 mag in 1990s). However, the orbital period is almost the same as it is now, taking into account a slow secular trend towards a faster orbital rotation. Thus, there is no evidence for an S Dor outburst. However, the triggering mechanism for the increased mass loss that started about a century ago is not clear.

As we mentioned in Sect. 1, parameters of RY Sct are similar to those of a large group of B[e]WD (currently ~50 objects). The group has the potential to become significantly larger, because of the large luminosity range of its objects (Sect. 1) and the fact that only the objects detected by IRAS and those with extremely strong emission-line spectra have been identified so far. The B[e]WD stars produce dust and a significant fraction of them seems to be binary systems (Miroshnichenko et al. 2002, 2005). Most of the group members are relatively low-luminosity objects ($L_\star \sim 10^3$–$10^4\,L_\odot$) and their mechanism of mass loss is not as well understood as that for the luminous stars, such as RY Sct (the radiatively-driven winds). Nevertheless, the noticeable amount of dust formed by RY Sct, together with a large expected number of B[e]WD members, suggest that they may be important dust producers in the Galaxy. It has been suggested that the luminous B[e] stars represent an evolutionary phase of massive stars, which also pass through Of, Ofpn/WN9, and LBV phases (Nota et al. 1996). Similarly, the B[e]WD phase may be inevitable for most stars with $M_\star \geq 3\,M_\odot$ or binaries with certain initial parameters. This makes B[e]WD stars very useful for a deeper understanding of the evolution of intermediate-mass and massive stars and of the dust formation processes. To make progress in this direction, infrared observations of these objects at both ground- and space-based facilities, such as the Keck telescope and the Spitzer Space Observatory, would be extremely important.

6. Conclusions

This paper presented the first detailed 2D radiative transfer modelling of the well-known eclipsing binary RY Sct and its dusty disc. We have performed an extensive exploration of the time-dependent model parameter space and accurate, self-consistent fitting of all existing observational data for the object, including its well-defined SED and high-resolution infrared images obtained at the Keck telescope at six infrared wavelengths, from 3 to 20 μm.

This radiative transfer modelling took into account all observational constraints from only *dust* continuum observations. Thus, by definition, our model of the dusty disc of RY Sct has ignored the gas component and all the complexities observed in the gas phase. The latter was approximately taken into account by the dust-to-gas mass ratio. Our goal was not to reproduce the extremely complex reality of the close binary system in its entirety (clearly impossible at this time), but instead to try and extract the best possible constraints on the physical properties of the system from the IR dust continuum observations. As a result of the modelling, a number of basic physical and geometrical parameters of this interesting object were derived with a better accuracy than before.

With the *effective* $T_\star = 27\,000$ K for both components and the distance $D = 1.8$ kpc, we derive the total luminosity of the binary $L_\star = 4.2 \times 10^5\,L_\odot$, much lower than in previous estimates and well below the Eddington luminosity. This luminosity is consistent with a lower mass of the binary (by a factor of ~2) than $M_\star \approx 80$–$90\,M_\odot$ sometimes suggested in the literature and strongly supports similar lower values (34–46 $M_\odot$, cf. Table 2) derived in several recent observational studies. The optically thin dusty disc with $\tau_V \approx 0.04$ in the equatorial plane extends from the inner boundary at $R_1 = 60$ AU to the outer radius $R_2 \approx 10^5$ AU, all the way into the interstellar medium. The high luminosity of the stars heats up even the interstellar dust, well beyond the outer boundary, to $T_\mathrm{d} \approx 100$ K. The large interstellar extinction $A_\mathrm{V} = 4.5$ mag towards RY Sct shapes its SED in the ultraviolet, optical and near infrared.

The disc with a full opening angle $\psi = 26°$ is observed at the viewing angle $\theta_v = 14°$ from its midplane (inclination $i = 76°$). The strong density enhancement in the disc within the narrow ring at $r = 1500$ AU emits most of the IR flux and is prominent in the Keck telescope images. Presumably the dense ring had been created by a fast wind that swept out and compressed the previously lost material in the older and slower stellar wind. The dust mass contained in the disc within $1''$ ($r = 1800$ AU) from the star is $m_d = 4.7 \times 10^{-7}\,M_\odot$, by a factor of 3 lower than in a recent estimate. However, there is ~ 30 times more mass in the surroundings of the binary system than within the dense ring. In fact, as much as 97% of the total dust mass $M_d = 9 \times 10^{-6}\,M_\odot$ (gas mass $M = 0.017\,M_\odot$) of the circumbinary material is contained within the outer, old wind.

Based on the fitting of the recent Keck telescope observations together with the old photometry, our model predicts that presently there is a relatively larger amount of small, hot dust grains in the dust formation zone, whose emission significantly changed the shape of the SED of RY Sct in the near IR. The hot dust density must now be higher in the dust formation zone, suggesting a higher mass-loss rate or dust-to-gas mass ratio or lower wind velocities than before, or a combination of these factors.

The fact that the nebula around RY Sct was resolved from the ground allows us to hope that similar structures might be resolved around other B[e]WD located closer to the Sun (e.g., HD 45677, HD 50138). However, such observations may require coronagrafic technique as other nebulae are relatively fainter, compared to the stars' brightness. New near-IR (*JHKL*) light curves would help us to understand the dust formation history in the RY Sct system. Spectral, photometric and imaging observations at longer wavelengths are very important to further constrain the dust chemical composition and the spatial extent of the envelope.

Acknowledgements. A.B.M. acknowledges support from the Natural Sciences and Engineering Research Council of Canada (NSERC) and A.S.M. acknowledges support from NASA grant NAG5–8054. We thank Nathan Smith for providing additional information about the Keck telescope images of RY Sct, Dieter Schertl for plotting the model images and Ian Short for the computation of the model atmospheres used in this work. We used the SIMBAD database operated at CDS, Strasbourg, France, and data products from the Two Micron All Sky Survey, which is a joint project of the University of Massachusetts and the Infrared Processing and Analysis Center/California Institute of Technology, funded by the National Aeronautic and Space Administration and the National Science Foundation. The work is also partly based on the INES data from the IUE satellite and the Keck telescope. The authors appreciate comments and suggestions of the anonymous referee that stimulated our work on further improvements of this paper.

References

Allen, D. A. 1973, MNRAS, 161, 145
Allen, D. A., & Swings, J.-P. 1976, A&A, 47, 293
Antokhina, E. A., & Cherepashchuk, A. M. 1988, Sov. Astron., 14, 105
Antokhina, E. A., & Kumsiashvili, M. I. 1999, Sov. Astron., 25, 662
Cardelli, J. A., Clayton, G. C., & Mathis, J. S. 1989, ApJ, 345, 245
Ciatti, F., Mammano, A., Margoni, R., et al. 1980, A&AS, 41, 143
Cowley, A. P., & Hutchings, J. B. 1976, PASP 88, 456
Cutri, R. M., Skrutskie, M. F., Dyk, S. V., et al. 2003, in 2MASS All-Sky Catalog of Point Sources (University of Massachusetts, Infrared Processing and Analysis Center/California Institute of Technology)
de Martino, D., Vittone, A. A., Rossi, C., & Giovanelli, F. 1992, A&A, 254, 266
Djurasevic, G., Zakirov, M., Eshankulova, M., & Erkapic, S. 2001, A&A, 374, 638
Draine, B. T. 1987, Princeton University Observatory Preprint, No. 213
Egan, M. P., Price, S. D., Kraemer, K. E., et al. 2003, in Air Force Research Laboratory Technical Report, Vol. AFRL–VS–TR–2003–1589
Gaposhkin, S. 1937, Ann. Harvard, 105, 509
Gehrz, R. D., Hayward, T. L., Houck, J. B., et al. 1995, ApJ, 439, 417
Gehrz, R. D., Smith, N., Jones, B., Puetter, R., & Yahil, A. 2001, ApJ, 559, 395
Giuricin, G., & Mardirossian, F. 1981, A&A, 101, 138
Grasdalen, G. L., Hackwell, J. A., Gehrz, R. D., & McClain, D. 1979, ApJ, 234, L129
IRAS PSC 1988, in The Point Source Catalog, Ver. 2.0, Vol. RP–1190, Infrared Astronomical Satellite Catalogs (NASA)
Jäger, C., Mutschke, H., & Henning, T. 1998, A&A, 332, 291
King, A. R., & Jameson, R. F. 1979, A&A, 71, 326
Koch, R. H. 1979, Inf. Bull. Variable Stars, 1580, 1
Kraus, M., & Lamers, H. J. G. L. M. 2003, A&A, 405, 165
Kurucz, R. L. 1993, Kurucz CD-ROM No. 13 (Cambridge: Smithsonian Astrophysical Observatory)
Lamers, H. J. G. L. M., Zickgraf, F. J., de Winter, D., Houziaux, L., & Zorec, J. 1998, A&A, 340, 117
Men'shchikov, A. B., & Henning, T. 1997, A&A, 318, 879
Men'shchikov, A. B., Hofmann, K.-H., & Weigelt, G. 2002, A&A, 392, 921
Milano, L., Vittone, A., Ciatti, F., et al. 1981, A&A, 100, 59
Miroshnichenko, A. S., Bjorkman, K. S., Chentsov, E. L., & Klochkova, V. G. 2002, in Exotic Stars as Challenges to Evolution, ed. C. A. Tout & W. V. Hamme (NASA), ASP Conf. Ser., 279, 303
Miroshnichenko, A. S., Levato, H., Bjorkman, K. S., & Grosso, M. 2003, A&A, 406, 673
Miroshnichenko, A. S., Levato, H., Bjorkman, K. S., et al. 2004, A&A, 417, 731
Miroshnichenko, A. S. et al. 2005, in Massive Stars in Interacting Binaries, ed. A. F. J. Moffat & N. Saint-Louis (NASA), ASP Conf. Ser., in press
Nota, A., Pasquali, A., Drissen, L., et al. 1996, ApJS, 102, 383
Sahade, J., Brandi, E., & Fontenla, J. M. 1984, A&AS, 56, 17
Sahade, J., West, R. M., & Skul'sky, M. Y. 2002, Rev. Mex. Astron. Astrofis., 38, 259
Savage, B. D., & Mathis, J. S. 1979, ARA&A, 17, 73
Schmutz, W., Leitherer, C., Hubeny, I., et al. 1991, ApJ, 372, 664
Short, C. I., & Hauschildt, P. H. 2005, ApJ, 618, 926
Smith, N., Gehrz, R. D., & Goss, W. M. 2001, AJ, 122, 2700
Smith, N., Gehrz, R. D., Humphreys, R., et al. 1999, AJ, 118, 960
Smith, N., Gehrz, R. D., Stahl, O., Balick, B., & Kaufer, A. 2002, ApJ, 578, 464
Strafella, F., Calamai, G., Fuensalida, J. J., Lorenzetti, D., & Saraceno, P. 1987, Mem. Soc. Astron. It., 58, 233
Volk, K., & Cohen, M. 1989, AJ, 98, 931
Williams, P. M., Kidger, M. R., van der Hucht, K. A., et al. 2001, MNRAS, 324, 156
Zakirov, M. M. 1985, Bull. Abastumanskaya Astrofiz. Obs., 58, 425